Lateral variation of the D″ discontinuity beneath the Cocos Plate

T. Lay
Earth Sciences Department, University of California, Santa Cruz, California, USA

E. J. Garnero
Department of Geological Sciences, Arizona State University, Tempe, Arizona, USA

S. A. Russell
Weston Geophysical Corporation, Lexington, Massachusetts, USA

Received 19 April 2004; revised 22 June 2004; accepted 2 July 2004; published 10 August 2004.

[1] Broadband shear wave signals from 15 deep South American earthquakes reveal small-scale variations of the D″ shear velocity discontinuity beneath the Cocos Plate. Deconvolution by average event source wavelets allows multiple event and California station combinations to be double-array stacked in 4 geographically separate reflection point bins with lateral dimensions of about 200 km. Reflections from the top of D″ are apparent in all 4 bins, with significant variations in timing and strength relative to ScS. The data are compatible with a discontinuous shear velocity increase 264 km above the core-mantle boundary that varies laterally in strength from 0.9% to 2.6%, with corresponding lateral velocity variations within D″. *INDEX TERMS:* 7203 Seismology: Body wave propagation; 7207 Seismology: Core and mantle; 8120 Tectonophysics: Dynamics of lithosphere and mantle—general; 8124 Tectonophysics: Earth's interior—composition and state (1212). **Citation:** Lay, T., E. J. Garnero, and S. A. Russell (2004), Lateral variation of the D″ discontinuity beneath the Cocos Plate, *Geophys. Res. Lett.*, *31*, L15612, doi:10.1029/2004GL020300.

1. Introduction

[2] The lowermost few hundred kilometers of the mantle is identified as the D″ region due to seismological evidence for inhomogeneity of the structure above the core-mantle boundary (CMB). An as-of-yet unexplained characteristic of D″ is the presence of rapid P and/or S velocity increases about 200 to 300 km above the CMB, which have been observed in many regions [e.g., *Wysession et al.*, 1998]. This feature is commonly called the D″ discontinuity. Thermal effects alone cannot account for the D″ discontinuity, and it is commonly attributed to either a compositional contrast or possibly a phase change [e.g., *Lay and Garnero*, 2004].

[3] Investigations of the D″ discontinuity at regional scales (e.g., ~200 km and less) are needed for progress to be made in understanding the nature of this structure. This is not viable for most of Earth's deep mantle given the limited distributions of suitable earthquake sources and seismic sensors. However, the lowermost mantle below the Caribbean and Central America is densely sampled by phases from South American earthquakes recorded at North American stations, and hence has been extensively studied. Past efforts indicate the presence of high shear velocities underlying a 2–3% velocity discontinuity 200–300 km above the CMB [e.g., *Lay and Helmberger*, 1983; *Kendall and Nangini*, 1996; *Garnero and Lay*, 2003]. A subregion west of Central America, located beneath the Cocos Plate, is particularly well-sampled by the dense short-period and broadband seismic networks in California, and prior studies have exploited this geometry to investigate both the P and S velocity structure in D″ [e.g., *Zhang and Lay*, 1984; *Ding and Helmberger*, 1997; *Reasoner and Revenaugh*, 1999; *Rokosky et al.*, 2004]. We apply double-array stacking [e.g., *Revenaugh and Meyer*, 1997] to a large data set of transverse component (SH) waves sampling this region, exploring small-scale lateral variations in D″ structure beneath the Cocos Plate.

2. Data and Methods

[4] We use SH ground displacements from 15 intermediate and deep focus South American events recorded by 49 broadband stations in California. Epicentral distances range between 64° to 83°. Horizontal component seismograms are deconvolved by their instrument responses, bandpass filtered (0.01/0.005–5 Hz), and then corrected for estimates of near-receiver lithospheric anisotropy [*Polet and Kanamori*, 2002] prior to rotation to the SH component. From 3 to 10 ScS arrivals for each event are aligned and stacked to produce average source wavelets with good signal-to-noise ratio. The source wavelets are deconvolved from the SH signals, with a 0.3 Hz lowpass Butterworth phaseless filter being applied. Figure 1 illustrates the advantage of the source wavelet deconvolution, as it isolates the discrete arrivals of interest: (a) the direct S phase, (b) the core-reflection ScS, and (c) the intermediate arrivals caused by triplication of the wavefield as it interacts with the D″ discontinuity, involving arrivals turning just below the discontinuity (Scd) and reflecting off the discontinuity (Sbc). The post-critical Sbc arrival is phase shifted, producing a small negative overshoot of the combined Scd + Sbc energy. In our distance range Sbc and Scd cannot be separately distinguished, and the combined arrival is called SdS. SdS phases could also arise from scattering from heterogeneities. The deconvolved filtered spike-trains are normalized in amplitude to have the ScS peak be unity, giving our final data form. A total of 255 signals with stable deconvolutions and

0094-8276/04/2004GL020300$05.00

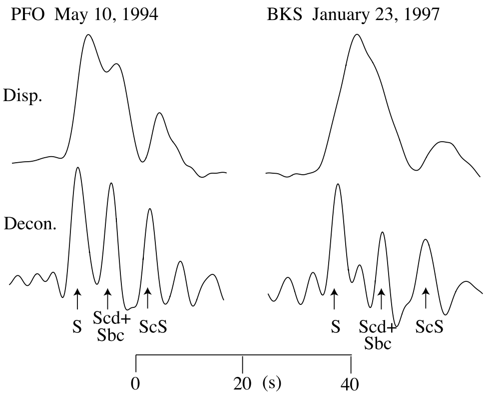

Figure 1. Examples of broadband SH displacements at stations PFO and BKS for two deep South American events. Instrument-corrected ground displacements (Disp.) are shown in the top row. The first arrival is S, and about 15–20 s later, ScS arrives. Deconvolution by the event-averaged source wavelets and low pass filtering below 0.3 Hz yields the spike-trains below for each record (Decon.). The intermediate arrival, Scd + Sbc (SdS), is clearly isolated in the deconvolutions.

good signal quality were retained for the double-array stacking.

3. Results

[5] Figure 2 shows a map of the ScS CMB reflection points: symbols indicate the visible presence or absence of a clear SdS arrival in the deconvolved signals. Almost all waveforms indicate some SdS energy, with the exception of a handful of signals with CMB reflection points between 4.5° and 7.5°N. The N-S distribution of reflection points stems from the distributions of Californian stations and events in the Peru-Bolivia-Argentina deep source regions. The raypaths trend from southeast to northwest, with little azimuthal coverage of the region (Figure 2).

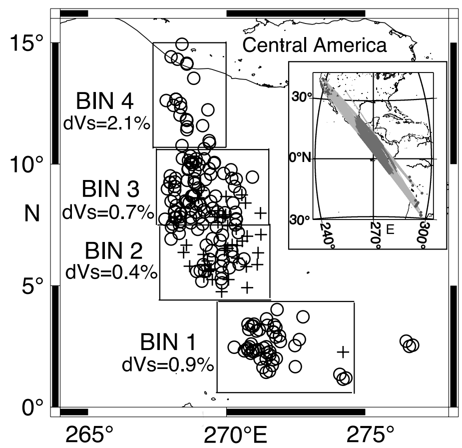

Figure 2. Map showing CMB reflection points for ScS phases for our data. Circles denote deconvolved waveforms for which we detect SdS between S and ScS by visual inspection, whereas plus signs indicate waveforms that lack a clear SdS phase. Boxes outline the four bins used for localized stacking. dVs denotes the average shear velocity anomaly in D″ for each bin from travel time analysis [*Rokosky et al.*, 2004]. Inset map shows source, receiver and raypath distributions with the dark portion of each ray indicating the path segment within a 250-km thick D″ layer.

[6] Initially, we stack all seismograms in a composite stack using all source-receiver combinations. Lateral variations in the actual velocity structure above the CMB will cause travel time fluctuations that degrade the stack coherency of any reflections from shallower depth. *Rokosky et al.* [2004] find a south-to-north increase in D″ shear velocities of several percent across our study area (see Figure 2). Thus, a single stack over the entire region should defocus any SdS energy. If the stacking velocity model is too slow on average, one might overestimate reflector depth, whereas if it is too fast on average, one might underestimate reflector depth.

[7] With this in mind, we use two reference velocity models: PREM [*Dziewonski and Anderson*, 1981], and a smoothed version of a D″ discontinuity model (SKNA2) obtained for Central America by *Kendall and Nangini* [1996], which we call SKNA2m (Figure 3). The latter model has higher average velocities than PREM over the lowermost 400 km of the mantle, consistent with the regional high velocities found in the northern portion of our study area in mantle tomography models [e.g., *Grand*, 2002]. Smoothing avoids triplication of the rays used for stacking. Figure 4 shows the double-array stacking results found using all 255 traces with PREM or SKNA2m as reference structures. The algorithm calculates times relative to ScS for precritical reflectors at various depths, and the traces are shifted and stacked, with the stack amplitude for each target depth being plotted [see *Revenaugh and Meyer*, 1997]. The normalized ScS arrivals stack coherently to give a unity peak at the CMB. Any energy that stacks at other depths is generically called SdS.

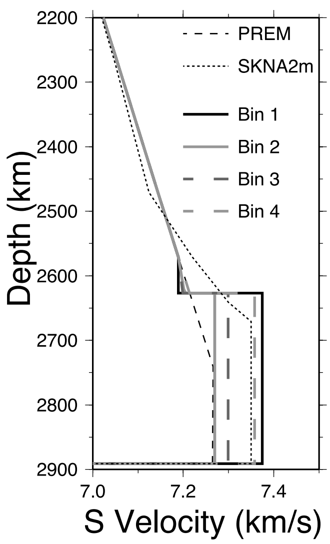

Figure 3. Velocity models obtained for each bin along with the two reference velocity structures PREM and SKNA2m used for stacking.

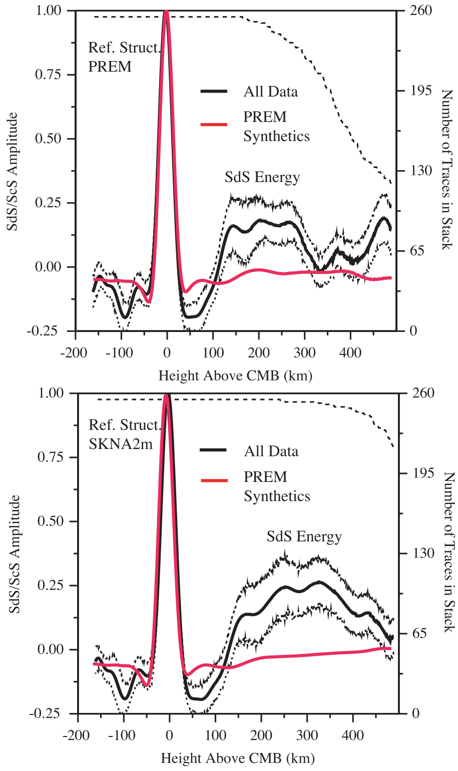

Figure 4. Double-array stacks of all 255 seismograms for two different reference velocity models, PREM (top) and SKNA2m (bottom). The amplitude of the stack at various target depths in the lower mantle is shown (bold lines), with bootstrap variances of the stack (dotted lines) as described by *Revenaugh and Meyer* [1997]. ScS stacks at the CMB. Short dashed lines indicate the number of traces contributing to the stack at each target depth (right scale). Red lines correspond to stacking of synthetics for model PREM, which has no SdS energy.

[8] For the PREM stack, a broad triplet feature is imaged at apparent depths of 100 to 300 km above the CMB. For the SKNA2m stack, the same broad feature appears 150 to 400 km above the CMB. The higher D″ velocities of the latter model yield shallower apparent depths for reflectors. The overlapping distribution of SdS energy in these composite stacks suggests spatial fluctuations in the timing of actual reflections. This is confirmed by subdividing the data set into 4 well sampled bins (Figure 2), and performing separate stacks. The bins were defined by the data distribution and the extent to which they separate SdS peaks at different apparent depths.

[9] Figure 5 shows the resulting stacks for the 4 bins with PREM being the reference model. Each bin displays a narrow SdS reflection horizon above the CMB, but there are variations in apparent depth and strength of the reflectors. The southernmost Bin 1 has a strong arrival, imaged 160 km above the CMB. Bin 2, just to the north in the region of Figure 2 where some traces lack visible arrivals between S and ScS, shows a weak SdS arrival, imaged 260 km above the CMB. The SdS arrival in Bin 3 is stronger than in Bin 2 and peaks around 240 km above the CMB, while in Bin 4, a strong feature peaks around 210 km above the CMB. Bin 4 suggests an additional coherent arrival, about 380 km above the CMB. Stacks for the 4 bins with SKNA2m as the reference model (not shown) contain similar SdS peaks, but at 60 to 80 km shallower apparent depths. Exploration of the precise binning yields abrupt changes, with two discrete peaks appearing when using bins that overlap those in Figure 2.

[10] Variation in amplitude of SdS, weakening with apparent height above the CMB, could be the result of reflection from a topographically varying surface with uniform velocity increase underlain by a high velocity D″. This requires about 100 km variation in the reflector depth over lateral scale-lengths of 200 km. In this scenario, the region with the shallowest discontinuity (Bin 2) should have the earliest ScS times because of the thickened high velocity layer. But, this is not consistent with the lateral shear velocity variations in this region inferred from ScS arrival times by *Rokosky et al.* [2004]. Another possibility is that lateral variations in the D″ velocity structure, which cause the ScS travel time anomalies, produce variations in apparent D″ reflector amplitude and height above the CMB.

[11] We model our stacks with synthetic seismograms using the reflectivity method of *Müller* [1985]. Synthetic seismograms are made for a large suite of 1D models involving simple sharp shear velocity discontinuities at various depths. The synthetics are deconvolved and stacked in the same manner as the data, to replicate any artifacts of the processing. We allow minimal structural variation above discontinuities with variable strengths, seeking to match the amplitude of the SdS feature in the data stacks. The velocity below the discontinuity was arbitrarily kept constant down to the CMB, as our data do not constrain the D″ velocity gradient. This model space yields a remarkably simple suite of models that fit the data well. Initial modeling resulted in 4 discontinuity structures at depths within 10 km of each other, with varying velocity

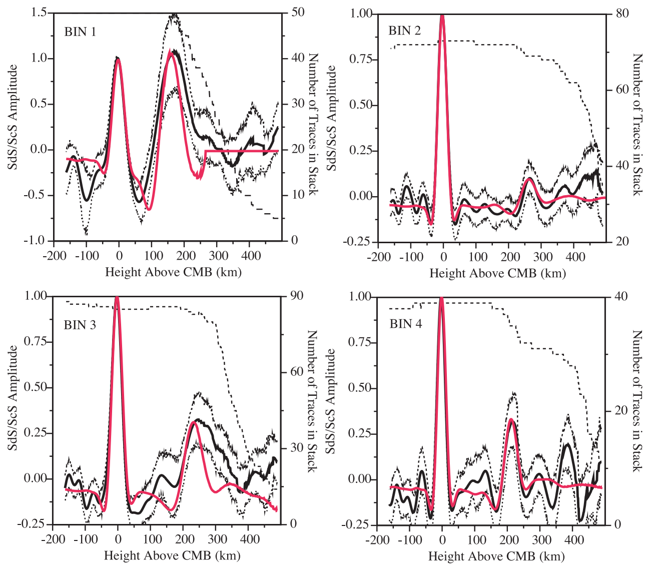

Figure 5. Data stacks for the four bins in Figure 2 following the format of Figure 4, with superimposed (red) stacks for synthetics for the preferred shear velocity models for each Bin (Figure 3).

increases. For our preferred models, we constrain the discontinuities to be at the same depth, 264 km above the CMB, making small adjustments to the velocity structures above and below the discontinuity.

[12] The final model profiles are shown in Figure 3, and the fit to the data is indicated in Figure 5. The shear velocity increases are 2.6% in Bin 1, 0.9% in Bin 2, 1.4% in Bin 3, and 2.0% in Bin 4. The timing and peak amplitude of the primary SdS peaks are well matched, including some of the negative downswing caused by Sbc phase shift, which images at depths below the SdS peaks. The synthetics fit the data equally well when both are stacked using the SKNA2m structure. The strength of the SdS energy in Figure 5 is not directly proportional to the size of the discontinuity because the data distance range involved in each stack varies: Bin 1 is dominated by data at large distances (>78°) where the triplication is very strong and ScS is weak, and Bin 2 is dominated by data at closer distances (<78°) where the triplication phases are weaker. This is accounted for in the modeling by using appropriate distance weighting.

[13] The extra energy at shallow depths in Bin 4 is not predicted, and could arise from a shallower discontinuity, but this feature is less apparent when we redo the entire analysis with a low pass filter of 0.2 Hz, so we are not confident in this secondary feature. It may involve coherent receiver coda from northern California stations, several of which have very complex SH signals. We also see some strong negative arrivals in individual waveforms from Bin 3, which do not stack coherently. These appear to be scattered arrivals from out-of-plane, and migration approaches are needed to image them [e.g., *Thomas et al.*, 2004].

4. Discussion and Conclusion

[14] The shear velocity models in Figure 3 are simply parameterized, and are not unique. There are close similarities to models previously obtained from California observations sampling the same region, but our analysis has provided unprecedented resolution of lateral variations in the shear velocity structure beneath the Cocos Plate. Stacking of short-period P data by *Reasoner and Revenaugh* [1999] suggests a similar pattern of a stronger P reflector in the southernmost region, weakening just to the north, then increasing toward the northern region, with variation in the PdP/P amplitude ratio of a factor of 1.7. Their modeling suggested depth fluctuations of from 162 to 218 km above the CMB, but there are again strong trade-offs between model parameterization and inferred discontinuity depth. Estimates of the P velocity contrast range from 0.4 to 0.6% for S velocity contrasts ranging from 0 to 3%, respectively. The estimated depths of the P and S discontinuities can easily be reconciled by changing the average velocities in either structure. The SH reflection coefficient does not depend on P velocity at all, and at the wide-angle geometries of our data there is almost no dependence on density contrast, which we assumed to be zero.

[15] The velocity structure within D″ in the models in Figure 3 is not constrained, and one could explore models in which the velocities converge at the CMB, while preserving the velocity jumps at the discontinuity. Doing so would require relative depth variations in the discontinuity between bins. For example, if the models for Bin 1 and Bin 2 are forced to converge at the CMB, the discontinuity in Bin 2 must be shallower than that in Bin 1. Many D″ velocity models include a negative gradient below the discontinuity, such as the model of *Ding and Helmberger* [1997] which is primarily for our Bin 1. Their model, with a 3% increase 200 km above the CMB and a strong negative gradient below the discontinuity, fits our data for Bin 1 quite well. However, the negative gradient was originally introduced to weaken strong post-critical diffractions, and is not needed when there are lateral variations in the structure, as implied by our results. Including a modest negative gradient has very minor affects on our models.

[16] Overall, we favor simple models of laterally varying average velocities in D″ that modulate the strength of the reflection from the top of D″. The strong northward increase in average velocity from Bin 2 to Bin 4 is very consistent with the strong lateral gradient to earlier ScS arrival times toward the north in the data of *Rokosky et al.* [2004], but the high velocity model for Bin 1 is not as clearly manifested in the ScS times (see Figure 2). This may be due to the relatively large distances of the signals sampling Bin 1, and the decreasing accuracy of tomographic models towards the south in this region. It is possible that the discontinuity is not laterally uniform, and that we are imaging scattered arrivals from discrete blobs of high velocity heterogeneity. Finer scale resolution and alternate model parameterizations such as migration [*Thomas et al.*, 2004] are needed to address this possibility. This study demonstrates that small scale variability exists on 100–200 km scalelengths within D″ and near the D″ discontinuity, presumably as a result of thermal and chemical variations. These observations provide challenges for chemical or phase change explanations of the discontinuity.

[17] **Acknowledgments.** Data were provided by the BDSN, Trinet and IRIS data centers. We thank J. Revenaugh for stacking software. Michael Wysession and an anonymous reviewer gave helpful suggestions. Supported by NSF grants EAR0125595 (T. L.) and EAR0135119 (E. J. G.). Contribution number 476 of the Center for the Study of Imaging and Dynamics of the Earth, IGPP, UCSC.

References

Ding, X., and D. V. Helmberger (1997), Modeling D″ structure beneath Central America with broadband seismic data, *Phys. Earth Planet. Inter.*, *101*, 245–270.

Dziewonski, A. M., and D. L. Anderson (1981), Preliminary reference Earth model, *Phys. Earth Planet. Inter.*, *25*, 297–356.

Garnero, E. J., and T. Lay (2003), D″ shear velocity heterogeneity, anisotropy, and discontinuity structure beneath the Caribbean and Central America, *Phys. Earth Planet. Inter.*, *140*, 219–242.

Grand, S. P. (2002), Mantle shear-wave tomography and the fate of subducted slabs, *Philos. Trans. R. Soc. London, Ser. A*, *360*, 2475–2491.

Kendall, J.-M., and C. Nangini (1996), Lateral variations in D″ below the Caribbean, *Geophys. Res. Lett.*, *23*, 395–402.

Lay, T., and E. J. Garnero (2004), *The State of the Planet*, *Geophys. Monogr. Ser.*, AGU, Washington, D. C., in press.

Lay, T., and D. V. Helmberger (1983), A lower mantle *S*-wave triplication and the shear velocity structure of D″, *Geophys. J. R. Astron. Soc.*, *75*, 799–837.

Müller, G. (1985), The reflectivity method: A tutorial, *J. Geophys.*, *58*, 153–174.

Polet, J., and H. Kanamori (2002), Anisotropy beneath California shear wave splitting measurements using a dense broadband array, *Geophys. J. Int.*, *149*, 313–317.

Reasoner, C., and J. Revenaugh (1999), Short-period *P* wave constraints on D″ reflectivity, *J. Geophys. Res.*, *104*, 955–961.

Revenaugh, J., and R. Meyer (1997), Seismic evidence of partial melt within a possibly ubiquitous low velocity layer at the base of the mantle, *Science*, *277*, 670–673.

Rokosky, J. M., T. Lay, E. J. Garnero, and S. A. Russell (2004), High-resolution investigation of shear wave anisotropy in D″ beneath the Cocos Plate, *Geophys. Res. Lett.*, *31*, L07605, doi:10.1029/2003GL018902.

Thomas, C., E. J. Garnero, and T. Lay (2004), High-resolution imaging of lowermost mantle structure under the Cocos Plate, *J. Geophys. Res.*, doi:10.1029/2004JB003013, in press.

Wysession, M. E., T. Lay, J. Revenaugh, Q. Williams, E. J. Garnero, R. Jeanloz, and L. H. Kellogg (1998), The D″ discontinuity and its implications, in *The Core-Mantle Boundary Region*, *Geodyn. Ser.*, vol. 28, edited by M. Gurnis et al., pp. 273–297, AGU, Washington, D. C.

Zhang, J., and T. Lay (1984), Investigation of a lower mantle shear-wave triplication using a broadband array, *Geophys. Res. Lett.*, *11*, 620–623.

E. J. Garnero, Department of Geological Sciences, Arizona State University, Tempe, AZ, USA.

T. Lay, Earth Sciences Department, University of California, 1156 High Street, Earth and Marine Sciences Building, Santa Cruz, CA 95064, USA. (tlay@es.ucsc.edu)

S. A. Russell, Weston Geophysical Corporation, Lexington, MA, USA.